Numerical simulation of electron cyclotron current drive characteristics on EAST*

Wei Wei(韦 维)[a)b)], Ding Bo-Jiang(丁伯江)[a)†], Zhang Xin-Jun(张新军)[a)], Wang Xiao-Jie(王晓洁)[a)], Li Miao-Hui(李妙辉)[a)], Kong Er-Hua(孔二华)[a)], and Zhang Lei(张 磊)[a)]

[a)] *Institute of Plasma Physics, Chinese Academy of Sciences, Hefei* 230031, *China*
[b)] *Hefei University of Technology, Hefei* 230009, *China*

(Received 28 August 2013; revised manuscript received 23 October 2013; published online 25 March 2014)

Electron cyclotron current drive (ECCD) will be applied in the EAST tokamak during its the new campaign. In order to provide theoretical predictions for relevant physical experiments, some numerical simulations of ECCD with the parameters of EAST have been carried out by using TORAY-GA code based on the understanding of ECCD mechanisms. ECCD efficiencies achieved in different plasma and electron cyclotron (EC) wave parameters are given. The dependences of ECCD characteristics on EC wave injection angle, toroidal magnetic field, plasma density, and temperature are presented and discussed.

Keywords: EAST, electron cyclotron current drive, current drive efficiency

PACS: 52.35.Hr, 52.55.Fa, 52.40.Fd, 52.65.Ff **DOI:** 10.1088/1674-1056/23/5/055201

1. Introduction

Electron cyclotron current drive (ECCD), an important type of non-inductive current drive, has many significant advantages compared with other methods of current drive. Its main advantages are easy coupling, strong localization, and controllable absorption. Its use is not only convenient for controlling the plasma current profile for the achievement of high-performance plasma, but also successful in suppressing the plasma MHD activity (sawtooth suppression, neoclassical tearing mode (NTM) suppression) to access high beta regimes. That is why ECCD is widely used as a useful tool in many fusion devices in the world. An experiment with ECCD to realize fully non-inductive current drive has been carried out on the TCV[1] tokamak. The synergy between ECCD and lower hybrid current drive (LHCD)[2] has been demonstrated in stationary conditions on Tore Supra.[3] ECCD is one of the main means of controlling MHD activity in ITER.[4] Stabilization of MHD by ECCD has been observed in HL-2A,[5,6] DIII-D,[7] JT-60U,[8] etc.

In EAST, a 140-GHz ECRH system aimed at high power and long pulse operation is under development and will be first put into use in the 2014 campaign. The main functions of this system on EAST would be: central electron heating (normalised radius $\rho < 0.3$), sawtooth control ($\rho \sim 0.3$), current profile control at mid-radius ($\rho \sim 0.5$–0.6), and NTM suppression ($\rho \sim 0.6$–0.75), and thus to develop high parameters and long pulse advanced plasma scenarios. It is required to heat or drive currents at various plasma minor radii to obtain the above objectives. Therefore, the first part of our research was focused mainly on the study of the current drive (CD) mechanism, efficiency, characteristics and its dependences on different parameters. It is necessary to calculate and predict some ECCD results for the new relevant experiments on EAST by using numerical simulation code.

Several significant simulation results are presented in this paper, which is organized as follows. The basic theory of ECCD and its mechanism, the estimate of CD efficiency, and the introduction of TORAY code are briefly introduced in Section 2. In Section 3, the effects of the main plasma and EC wave parameters on ECCD characteristics are highlighted. Finally, a conclusion is given in Section 4.

2. ECCD theory and TORAY code

In order to understand the ECCD mechanism, the resonance condition for wave-particle interaction in velocity space must be analyzed, which is given by the following equation:[9]

$$\omega = n\omega_{\rm ce}/\gamma + k_{\parallel} v_{\parallel}, \tag{1}$$

where ω is the wave frequency, $\omega_{\rm ce}$ is the electron cyclotron frequency, n is the electron harmonic number, $\gamma = 1/\sqrt{1-(v^2/c^2)}$ is the relativistic form-factor, which is a consequence of the relativistic correction of the electron mass, c is the velocity of light in vacuum. The $k_{\parallel} v_{\parallel}$ term is the Doppler effect, which plays an important role in ECCD and causes both shift and broadening of the absorption line, where $v_{\parallel}$, $k_{\parallel}$ are the parallel components of the velocity of the resonant electrons and wave vector of the EC wave, respectively. The EC wave interacts only with those electrons with the parallel velocity satisfying this electron cyclotron resonance condition. This interaction causes resonant electrons to obtain energy from the

*Project supported by the National Magnetic Confinement Fusion Science Program of China (Grant No. 2011GB102000) and the National Natural Science Foundation of China (Grant Nos. 11175206 and 11305211).

†Corresponding author. E-mail: bjding@ipp.ac.cn

© 2014 Chinese Physical Society and IOP Publishing Ltd

EC wave and leads to an increase of the transverse velocity of these resonant electrons. Then the total electron velocity increases, the collision frequency decreases, and the free-pass time of these electrons increases. It will lead to deviations of the electron distribution from Maxwell distribution in the velocity space and finally form an asymmetric electron distribution function, which drives plasma current during the EC wave application.

ECCD efficiency, according to Ref. [10], can be written in the form

$$\gamma_{\mathrm{ECCD}} = \frac{I_{\mathrm{EC}}}{P_{\mathrm{EC}}} = \zeta \times \frac{T_{\mathrm{e}}}{n_{\mathrm{e}} R(z_{\mathrm{eff}}+5)}, \tag{2}$$

where ζ is the normalized CD efficiency, which depends on the parameters of the EC wave and ECCD geometry, n_{e} is the electron density, T_{e} is the electron temperature, R is the major radius of the plasma, and Z_{eff} is the effective charge.

Another definition for the CD efficiency often used in engineering is[11]

$$\eta_{\mathrm{ECCD}} = \frac{I_{\mathrm{ECCD}} n_{\mathrm{e}} R}{P_{\mathrm{ECRH}}} \quad (\mathrm{A\cdot m^{-2}\cdot W^{-1}}), \tag{3}$$

where I_{ECCD} is the total driven current, n_{e} is in units of 10^{20} $\mathrm{m^{-3}}$, P_{ECRH} is the absorbed power of EC wave. Equation (3) does not contain the temperature effect, but it is more useful as an experimental estimation method to compare with the CD efficiency in different machines. The maximal CD efficiency η_{ECCD} achieved in T-10[12] experiments was 0.013×10^{20} $\mathrm{A\cdot m^{-2}\cdot W^{-1}}$, and the predicted ECCD efficiency η_{ECCD} in ITER[10] can be achieved as high as 0.3×10^{20} $\mathrm{A\cdot m^{-2}\cdot W^{-1}}$.

In addition, in order to achieve the driven current, the electron distribution function affected by EC wave must be obtained firstly, and then the driven current can be calculated according to the electron distribution function. Ignoring a static parallel electric field and including the effects of Coulomb collisions, and EC waves, the Fokker–Planck equation is written symbolically as follows:[13,14]

$$\frac{\partial f}{\partial \tau} = \left(\frac{\partial f}{\partial \tau}\right)_{\mathrm{EC}} + \left(\frac{\partial f}{\partial \tau}\right)_{\mathrm{C}}, \tag{4}$$

where $f = f(u_{\parallel}, u_{\perp}, r, t)$ is the electron distribution function at the radial location r and at time t, $u_{\parallel}$ and $u_{\perp}$ are the components of $\boldsymbol{u} \equiv \boldsymbol{p}/\sqrt{m_{\mathrm{e}} T_{\mathrm{e}}}$ respectively parallel and perpendicular to the ambient magnetic field, where $\boldsymbol{p}$ is the electron momentum, $\boldsymbol{u}$ is the normalized momentum with m_{e} the electron mass and T_{e} the electron temperature, $\tau \equiv \nu_{\mathrm{e}} t$ is the time in terms of the collision period ν_{e}^{-1}, $(\partial f_{\mathrm{e}}/\partial\tau)_{\mathrm{EC}}$ is the diffusion term caused by EC wave, it can be expressed as[15]

$$\left(\frac{\partial f_{\mathrm{e}}}{\partial \tau}\right)_{\mathrm{EC}} = \frac{\partial}{\partial \boldsymbol{u}} \cdot D_{\mathrm{EC}} \cdot \frac{\partial f}{\partial \boldsymbol{u}}, \tag{5}$$

where D_{EC} is the EC diffusion coefficient in momentum space, which can be found in Ref. [16]. Equation (4) indicates that the diffusion term results in the deviation of electron velocity distribution from thermal equilibrium distribution and leads to an asymmetric distortion, $(\partial f_{\mathrm{e}}/\partial\tau)_{\mathrm{C}}$ is the collision term, which represents the effect of Coulomb collision on velocity distribution function. It tends to make any deviation from thermal equilibrium distribution return to Maxwell distribution in the collision time scale. i.e., eliminate the distortion. Combining the two terms above, a steady distortion distribution (i.e., a asymmetric electron distribution function) can be formed and the non-inductive current can be driven continually during the EC wave application.

Once the electron distribution function is obtained, the driven current density associated to f can be calculated by[13]

$$J = -e \int v_{\parallel} f \, \mathrm{d}^3 v. \tag{6}$$

The codes used most often by solving the Fokker–Planck equation in the quasi-linear approximation to obtain wave absorption and current drive are TORAY, CQL3D,[17] REMA, C3PO/LUKE,[18] etc. The code used in this study is TORAY-GA (TORAY for short) code. TORAY code[19,20] is a ray tracing code which treats the transmission of EC wave as a Gauss beam, and combines with the Fokker–Planck equation to solve the power deposition and current drive in a wave propagation process. By mean of the code simulation, power deposition and current profile can be obtained. In this paper, plasma equilibrium is simulated by EFIT code. The profile of electron density n_{e}, electron temperature T_{e}, and effective charge number Z_{eff} with normalized minor radius ρ as shown in Fig. 1, are assumed to have parabolic distribution.

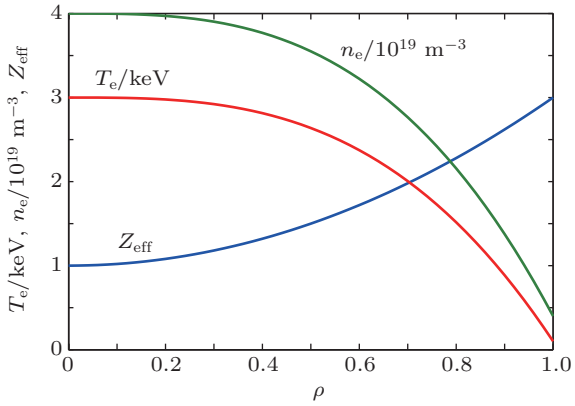


Fig. 1. (color online) Radial profiles of electron density, electron temperature, and effective charge number used in this paper.

3. Results of numerical simulation

3.1. Main parameters of EAST device and ECRH system

EAST is a full superconducting tokamak device with a non-circular cross section. The typical background plasma parameters are as follows: plasma major radius $R = 1.85$ m, plasma minor radius $a = 0.45$ m, plasma current $I_{\mathrm{P}} = 1$ MA, plasma elongation ratio $\kappa = 1.9$, and triangle variable factor $\delta = 0.5$. In the next few years, the operational objective of

toroidal magnetic field (B_0) on EAST is 2.5 T. Based on the relationship of wave frequency and toroidal magnetic field, $f = 28nB_0$ (where f and n are EC wave frequency and electron harmonic number, respectively), choosing the maximum magnetic field $B_0 = 2.5$ T, the working frequency of the ECRH system is chosen to be 140 GHz and the second harmonic extraordinary mode (X2) is used for electron heating and current drive. The wave source consists of four gyrotrons with each 1 MW/1000 s output power. A total of 4-MW power is injected into the plasma through the horizontal port from the low field side.

3.2. Effects of launch angle on ECCD characteristics

In order to change the power deposition of the EC wave at different magnetic surfaces and achieve different physical functions, one of most common methods is to adjust poloidal or toroidal incident angles of the EC wave antenna by using a movable mirror. The definition of EC wave incident angle is shown in Fig. 2, in which θ and φ refer to poloidal angle and toroidal angle, respectively.

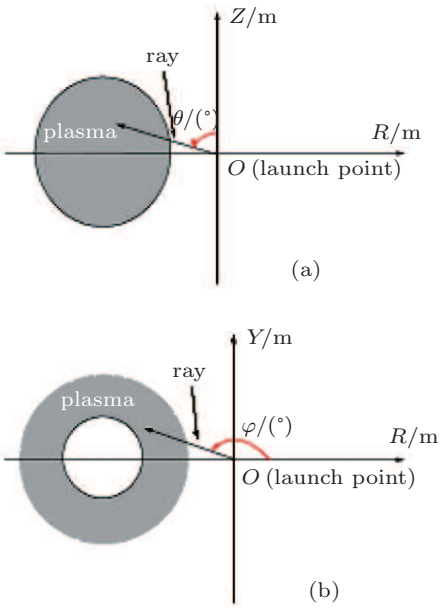


Fig. 2. The rotation angle of incident beam (φ: toroidal angle, θ: poloidal angle). (a) Poloidal cross section of tokamak and (b) toroidal cross section of tokamak.

ECCD characteristics with different poloidal and toroidal angles are shown in Fig. 3 with the following parameters: $B_0 = 2.2$ T, the radius of the launch point of the EC wave $R_a = 300$ cm, and the vertical deviation of the launch point with respect to the middle plane $Z_a = 30$ cm. It can be seen from Figs. 3(a) and 3(c) that the effect of poloidal angle on driven current density and its radial position is obvious. The poloidal angle of 100°–105° is the boundary, which can make the beams propagate to the plasma center because Z_a has a certain height. As the poloidal angle increases or decreases out of this range, the position of the peak current density changes from the normalized minor radius ρ of 0.03 to 0.82, i.e., the current basically can be driven by EC wave from the core to the edge of the plasma.

On the other hand, the dependence of total driven current on toroidal angles is sensitive, as shown in Fig. 3(b). When the toroidal angle equals 180°, i.e., vertical injection of EC wave into plasma, the drive efficiency becomes very poor. With the increase of the toroidal incident angle, the drive efficiency becomes better and reaches the maximum at the toroidal angle of about 205° and poloidal angle ranging from 100° to 105°. The maximum driven current is 33 kA/MW when the electron density is 0.24×10^{20} m^{-3} and center electron temperature is 3 keV. Based on Eq. (3), the maximum CD efficiency on EAST can be obtained as 0.015×10^{20} A·m^{-2}·W^{-1}. A high CD efficiency related to a larger toroidal rotation angle can be interpreted by the electron cyclotron resonance condition. We can conclude from Eq. (1) that if the toroidal launch angle of the EC wave is oblique, the value of $k_{\|}$ becomes larger, and the parallel velocity of electrons becomes smaller because of the equation, $v_{\|} = (\omega - n\omega_{ce})/k_{\|}$, which means that more electrons with lower energy in parallel direction can obtain energy from the EC wave and more current can be driven. Furthermore, a larger $k_{\|}$ means a more obvious Doppler effect, leading to the outward shift of the resonant location of the electron, the flight direction of which is consistent with the propagation direction of the EC wave. Therefore, it is obvious that with the increase of φ ($180° < \varphi < 205°$ when $B_0 = 2.2$ T), the driven current not only increases but also moves to the plasma center, as shown in Figs. 3(b) and 3(c). However, if φ is too large, the resonant absorption position may have moved to the low field side because of the Doppler effect; where the electron temperature is lower, the collision frequency is larger and the trapped particles increase, which will lead to a decrease of CD efficiency. That is why when φ is larger than 210°, the driven current density and total driven current begin to decline and the profile of driven current becomes broad rapidly.

In addition, for MHD suppression, the width of the driven current profile is also a key parameter. Many experimental results indicate that the MHD instabilities can only be controlled when the width of the driven current profile is narrower than the minimum size of the magnetic island. Figure 3(d) shows the corresponding relationship between the incident angle and the $1/e^2$ width of the peak current density, which indicates the degree of localization of the driven current profile. It is seen that when the toroidal rotation angle is small, the width of the current density profile is small, i.e., a good localization of the driven current related to a smaller toroidal angle of EC wave, the reason for which may also be associated with the Doppler effect. As mentioned above, the Doppler effect, which is affected by toroidal angle, can cause the broadening of the absorption line and affect the absorption width of the power deposition.

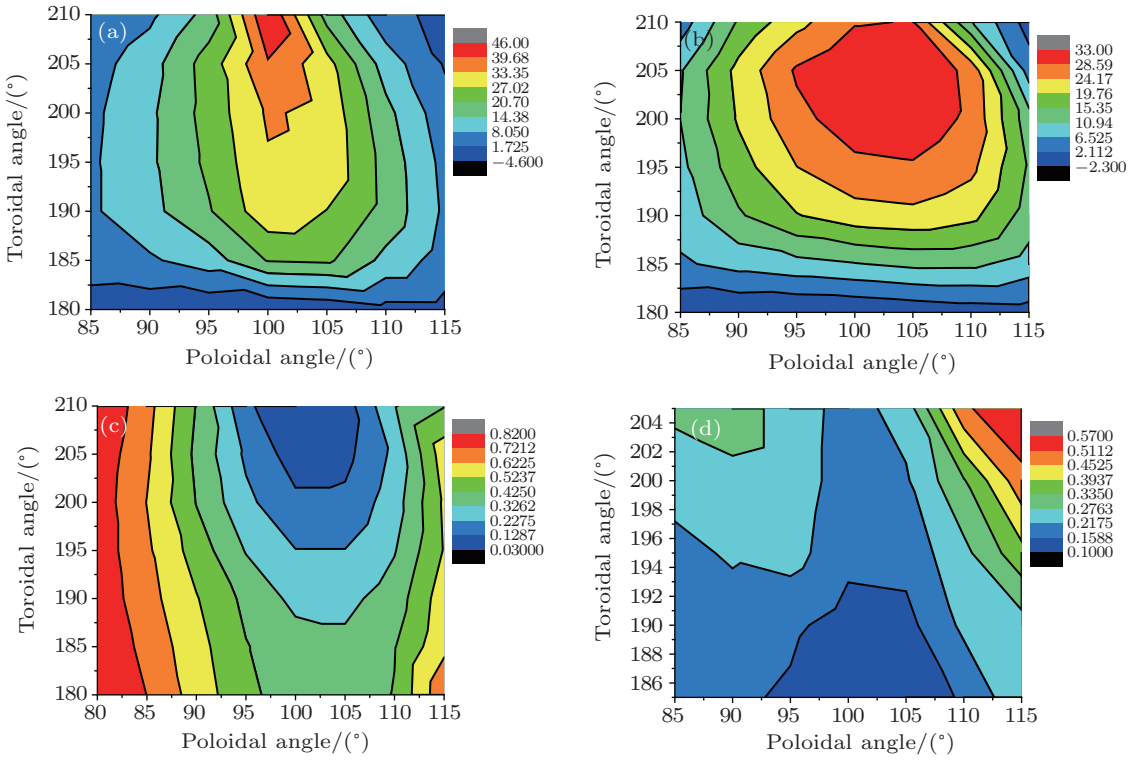


Fig. 3. Two-dimensional variation of ECCD characteristics with different poloidal and toroidal angles when $B_0 = 2.2$ T, $R_a = 300$ cm, and $Z_a = 30$ cm. (a) Driven current density in units of A·cm^{-2}·MW^{-1}, (b) total driven current in units of kA·MW^{-1}, (c) radial position of the peak current density, and (d) full width of ρ contours containing $1/e^2$ of the current density.

3.3. Effects of toroidal magnetic field on ECCD characteristics

In order to understand the operational diagram of the ECCD system on EAST, as shown in Table 1, the CD characteristics at different poloidal angles (from 80° to 115°, with interval of 5°) and toroidal angles (from 180° to 210°, with interval of 5°) have been investigated by scanning the toroidal magnetic field B_0 (2.0 T, 2.2 T, 2.3 T, 2.4 T, 2.5 T, 2.6 T) with $R_a = 300$ cm and $Z_a = 30$ cm. The conclusions are summarized as follows: firstly, when $B_0 = 2.2$ T–2.6 T, EC wave power can be deposited over a wide range with ρ varying between 0 and 0.75, satisfying each physical objective by the ECCD system on EAST; secondly, the CD efficiency at 2.0 T is poor and can be improved by increasing the magnetic field B_0 from 2.0 T to 2.6 T. When B_0 equals to about 2.5 T, the CD efficiency is the best. It is because the effect of toroidal field on resonance is very strong (see Fig. 4). It is found that with the increase of the toroidal field, the resonant layer moves from the high field side to the low field side gradually. The resonant layers locate at $\rho \sim 0.5$–0 in the high field side when $B_0 = 2.2$ T–2.6 T. As we know, the resonance occurring on the central axis can heat and drive on-axis current efficiently because of the higher temperature on the central axis. Furthermore, resonance on the high field side may result in core CD because of the Doppler effect. However, the resonant layer at higher B_0 ($B_0 > 2.6$ T, for 140 GHz EC wave frequency) will locate at the plasma edge of the low field side, where a higher fraction of trapped electrons will decrease the CD efficiency.[21,22] Therefore, it is important to optimize the toroidal magnetic field for realization of the physical objective. Finally, it can be inferred from Table 1 that with the increase of toroidal magnetic field, the optimal toroidal angle for the acquisition of the best CD efficiency decreases, and the optimal poloidal angle increases gradually. It is possibly relevant to the different locations of resonant layer when the toroidal field is different.

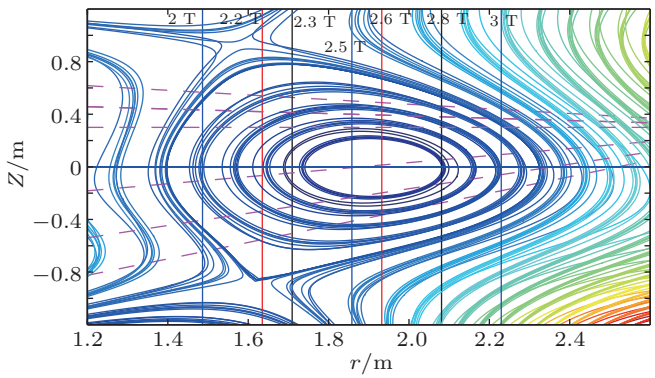


Fig. 4. (color online) The second harmonic electron cyclotron resonances for 140 GHz at different toroidal magnetic fields on EAST.

Table 1. The effects of different toroidal magnetic fields on the current drive. Here, $\Delta\rho$ is the radial range of EC power that can be deposited, I_{max} is the maximum total current driven by EC wave, I_{dmax}, ρ, and (φ, θ) are the maximum current density, its corresponding radial position and injection angle of the EC wave antenna, $\Delta\varphi$ and $\Delta\theta$ are the incident angle range for the best CD efficiency.

B_0/T	$\Delta\rho$	I_{max}/kA·MW^{-1}	η_{ECCD}/A·m^{-2}·W^{-1}	I_{dmax}/A·cm^{-2}·MW^{-1}	ρ	(φ, θ)	$\Delta\varphi$	$\Delta\theta$
2.0	0.42–0.9	24	0.011×10^{20}	10	0.42	(205°, 100°)	200°–205°	100°–105°
2.2	0.04–0.82	33	0.015×10^{20}	50	0.03	(210°, 100°)	195°–205°	100°–105°
2.3	0–0.81	34	0.015×10^{20}	80	0.03	(205°, 100°)	195°–205°	100°–105°
2.4	0–0.79	34	0.015×10^{20}	120	0.02	(195°, 100°)	195°–205°	100°–105°
2.5	0–0.76	31	0.014×10^{20}	120	0.01	(195°, 105°)	190°–200°	100°–110°
2.6	0–0.74	27	0.012×10^{20}	130	0.02	(190°, 105°)	190°–195°	100°–110°

The achievement of different physical objectives requires the ECCD system to drive current at various plasma minor radii. A higher driven current density sometimes is more important than the total current when ECCD is used to control the MHD activity. Experiments indicated that the NTM stabilization was observed when the driven current density exceeds the bootstrap current density at the rational surface.[23,24] Therefore, as shown in Table 2, the maximum current density in relevant minor radii and their corresponding radial positions and incident angles in $B_0 = 2.2$ T, 2.3 T, 2.4 T, 2.5 T, 2.6 T are investigated when EC wave is applied for saw tooth control, q control at mid-radius, 3/2 NTM control, 2/1 NTM control. Table 2 also shows the strong decrease of CD efficiency when the layer of absorption moves towards an off-axis location in any toroidal field, particularly on the low field side, owing to the effect of trapped electrons.

Table 2. Characteristic comparison of various functions by ECW in different toroidal magnetic fields.

B_0/T	sawteeth control $\rho = 0.3$			q control at mid-radius $\rho = 0.5$			3/2 NTM control $\rho = 0.6$			2/1 NTM control $\rho = 0.7$		
	I_{dmax} /A·cm^{-2}·MW^{-1}	ρ	(φ, θ)	I_{dmax} /A·cm^{-2}·MW^{-1}	ρ	(φ, θ)	I_{dmax} /A·cm^{-2}·MW^{-1}	ρ	(φ, θ)	I_{dmax} /A·cm^{-2}·MW^{-1}	ρ	(φ, θ)
2.2	34	0.3	(190°, 105°)	13	0.48	(200°, 90°)	7	0.62	(200°, 85°)	5	0.69	(185°, 85°)
2.3	21	0.3	(190°, 95°)	11	0.48	(190° ,90°)	6	0.6	(200°, 85°)	4	0.68	(185°, 85°)
2.4	12	0.3	(195°, 115°)	7	0.55	(195°, 85°)	6	0.58	(200°, 85°)	2	0.71	(190°, 80°)
2.5	13	0.33	(190°, 90°)	7	0.53	(190°, 85°)	4	0.61	(205°, 85°)	2	0.69	(190°, 80°)
2.6	18	0.29	(200°, 95°)	5	0.5	(205°, 90°)	4	0.59	(195°, 85°)	1	0.69	(190°, 80°)

3.4. Effects of electron density and temperature on ECCD characteristics

The ECCD characteristics and efficiency are different with different electron densities and at different temperatures. Figures 5 and 6 compare the effects of different electron densities and temperatures on ECCD. It shows that when the electron density and electron temperature are in the range of 1.0×10^{19} m^{-3}–8.0×10^{19} m^{-3} and 1 keV–10 keV, respectively, the driven current is proportional to the electron temperature and inversely proportional to the electron density. The calculated results by TORAY are in close agreement with the theoretical value by linear fitting. The reason why the electron density can affect the driven current is related to the Fokker–Planck equation. According to Eq. (4), an increase of electron density will lead to an increase of particle collision frequency, which will offset the effect of diffusion term, and hence the EC wave-driven current will decrease. In addition, the CD efficiency gets better with the increase of the electron temperature because the higher temperature means the higher velocity of resonant electrons and the lower collision frequency. Moreover, more electrons can interact with the wave.

Figure 7 shows the two-dimensional variation of ECCD characteristics with electron density and temperature. It can be seen from Figs. 7(a) and 7(b) that with the increase of the electron density, the driven current density and total driven current decrease gradually, however, with the increase of the electron temperature, the driven current density and total driven current increase obviously. Therefore, in order to obtain a higher driven current, the experiments should be carried out in a lower density and a higher temperature. However, as shown in Fig. 7(c), a higher CD efficiency calculated by

$$\eta_{ECCD} = \frac{I_{ECCD} n_e R}{P_{ECRH}} \quad (\mathrm{A\cdot m^{-2}\cdot W^{-1}})$$

is obtained at the higher T_e and n_e values. This is mainly because of the increase of T_e and n_e, i.e., the electron pressure rises, leading to an effective weakening of the trapping effect. Indeed, the EC wave launched from low field side will be absorbed farther from the resonance layer at the higher T_e and n_e, which can shift the resonance region farther from trapped passing boundary. In addition, it is found from Fig. 7(d) that the radial position of the peak current density moves to the plasma center, with the increase of the electron density and temperature. Especially, in a lower electron temperature, the position of the peak current density is more sensitive to the electron temperature, and not sensitive to the electron density.

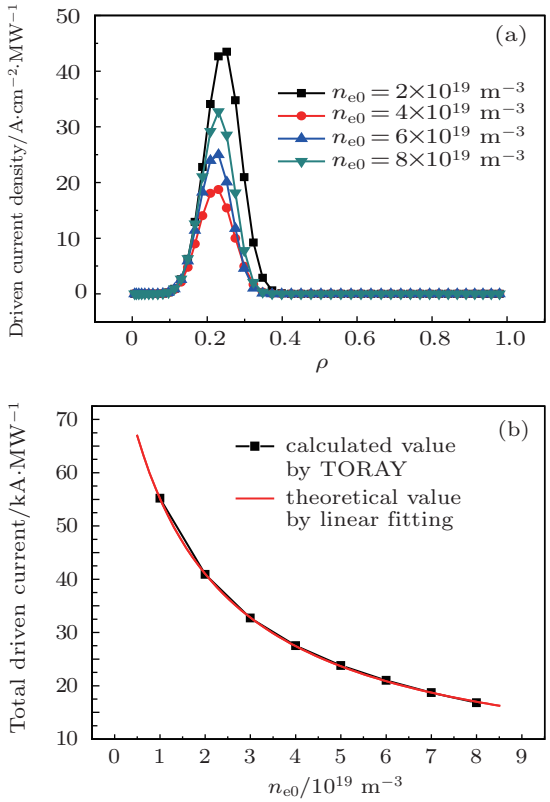


Fig. 5. (color online) ECCD characteristics of different electron densities with $B_0 = 2.2$ T, $R_a = 300$ cm, $Z_a = 30$ cm, $\varphi = 195°$, $\theta = 100°$, and $T_{e0} = 3$ keV (where n_{e0} is the center electron density).

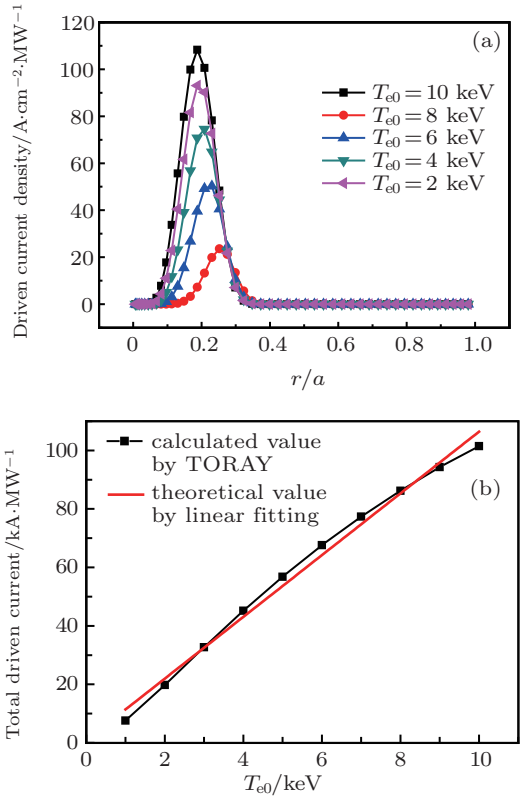


Fig. 6. (color online) ECCD characteristics of different electron temperatures with $B_0 = 2.2$ T, $R_a = 300$ cm, $Z_a = 30$ cm, $\varphi = 195°$, $\theta = 100°$, and $n_{e0} = 3.0\times10^{19}$ m^{-3} (T_{e0} is the center electron temperature).

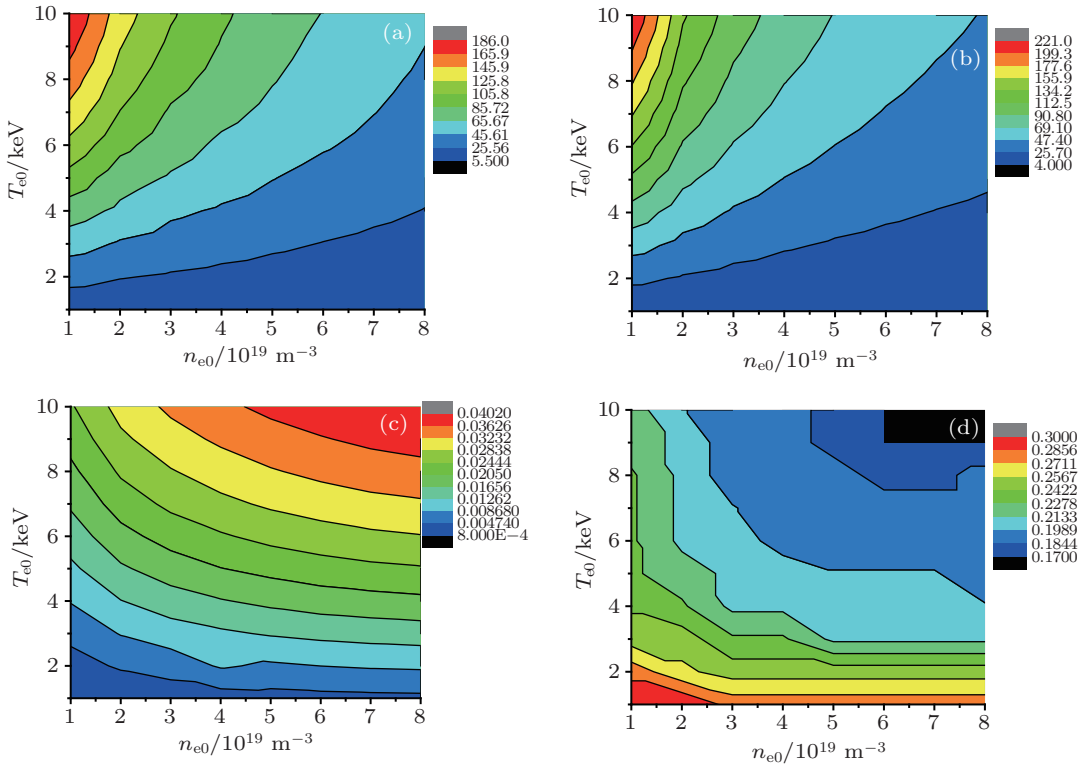


Fig. 7. Two-dimensional variation of ECCD characteristics with different electron densities and electron temperatures when $B_0 = 2.2$ T, $R_a = 300$ cm, $Z_a = 30$ cm, $\varphi = 195°$, and $\theta = 100°$. (a) Driven current density in units of A·cm^{-2}·MW. (b) Total driven current in units of kA·MW^{-1}. (c) CD efficiency η_{ECCD} in units of 10^{20} A·m^{-2}·W^{-1}. (d) Radial position of the peak current density.

4. Conclusion

Numerical simulation of ECCD has been systematically done and investigated by using TORAY in EAST. By means of the simulation, we have shown that poloidal angle and toroidal angle affect power deposition and driven current obviously, hence, getting a strong localized current density with a smaller toroidal rotation angle and a high CD efficiency with a larger toroidal angle. Simulation results with different incident angles will be useful for different physics objectives. Secondly, the ideal toroidal field for ECCD in EAST is the one that yields a resonant layer located on the high field side, at $\rho \sim 0.5$–0, where the electron temperature is higher and the fraction of trapped electrons is reduced. Finally, in a certain range of electron density (less than 8.0×10^{19} m^{-3}) and temperature (less than 10 keV), the driven current is proportional to the electron temperature and the inversely proportional to electron density. Furthermore, a higher CD efficiency is obtained at the higher T_e and n_e values. All these results provide an effective tool for future experiments relevant to ECCD on EAST.

References

[1] Coda S, Goodman T P, Henderson M A, *et al.* 2000 *Plasma Phys. Control. Fusion* **42** B311

[2] Hong B B, Chen S Y, Tang C J, Zhang X J and Hu Y J 2012 *Acta Phys. Sin.* **61** 115207 (in Chinese)

[3] Giruzzi G, Artaud J F, Dumont R J, Imbeaux F, Bibet P, Berger-By G, Bouquey F, Clary J, Darbos C, Ekedahl A, Hoang G T, Lennholm M, Maget P, Magne R and Se'gui J L 2004 *Phys. Rev. Lett.* **93** 255002

[4] Omori T, Henderson M A, Albajar F, *et al.* 2011 *Fusion Engineering and Design* **86** 951

[5] Duan X R, Ding X T, Dong J Q, *et al.* 2009 *Nucl. Fusion* **49** 104012

[6] Gong X Y, Peng X W, Xie A P and Liu W Y 2006 *Acta Phys. Sin.* **55** 1307 (in Chinese)

[7] Prater R, La Haye R J, Lohr J, Luce T C, Petty C C, Ferron J R, Humphreys D A, Strait E J, Perkins F W and Harvey R W 2003 *Nucl. Fusion* **43** 1128

[8] Nagasaki K, Isayama A, Ide S and JT-60 team 2003 *Nucl. Fusion* **43** L7

[9] Erckmann V and Gasparino U 1994 *Plasma Phys. Control. Fusion* **36** 1869

[10] Kirneva N A 2001 *Plasma Phys. Control. Fusion* **43** A195

[11] Poli E, Tardini G, Zohm H, Fable E, Farina D, Figini L, Marushchenko N B and Porte L 2013 *Nucl. Fusion* **53** 013011

[12] Esipchuk Y V 1995 *Plasma Phys. Control. Fusion* **37** A267

[13] Lin-Liu Y R, Chan V S and Prater R 2003 *Phys. Plasmas* **10** 4064

[14] Krivenski V, Fidone I, Giruzzi G and Granata G 1985 *Nucl. Fusion* **25** 127

[15] Dumont R J and Giruzzi G 2004 *Phys. Plasmas* **11** 3449

[16] Da S Rosa P R and Ziebell L F 2002 *Plasma Phys. Control. Fusion* **44** 2065

[17] Harvey R W and McCoy M G 1992 *IAEA Conf. Proc., Technical Committee Meeting on Advances in Simulation and Modeling of Thermonuclear Plasmas*, June 15, 1992, Montreal, Canada, p. 527

[18] Artaud J F, Basiuk V, Imbeaux F, *et al.* 2010 *Nucl. Fusion* **50** 043001

[19] Mazzucato E, Fidone I and Granata G 1987 *Phys. Fluids* **30** 3745

[20] Prater R, Farina D, Gribov Y, Harvey R W, Ram A K, Lin-Liu Y R, Poli E, Smirnov A P, Volpe F, Westerhof E, Zvonkov A and the ITPA Steady State Operation Topical Group 2008 *Nucl. Fusion* **48** 035006

[21] Petty C C, Lin-Liu Y R, Luce T C, Makowski M A, Prater R, Schuster D I, St. John H E and Wong K L 2001 *Nucl. Fusion* **41** 551

[22] Jiao Y M, Long Y X, Dong J Q, Gao Q D, Wang A K and Liu Y 2007 *Chin. Phys. B* **16** 3464

[23] Isayama A, Kamada Y, Ide S, Hamamatsu K, Oikawa T, Suzuki T, Neyatani Y, Ozeki T, Ikeda Y, Kajiwara K and the JT-60 team 2000 *Plasma Phys. Control. Fusion* **42** L37

[24] Zohm H, Gantenbein G, Gude A, Günter S, Leuterer F, Maraschek M, Meskat J, Suttrop W, Yu Q and ASDEX Upgrade Team and ECRH-Group 2001 *Phys. Plasmas* **8** 2009